

## Reconstruction of three-dimensional ozone fields using POAM III during SOLVE

C. E. Randall,<sup>1</sup> J. D. Lumpe,<sup>2</sup> R. M. Bevilacqua,<sup>3</sup> K. W. Hoppel,<sup>3</sup> M. D. Fromm,<sup>2</sup> R. J. Salawitch,<sup>4</sup> W. H. Swartz,<sup>5,6</sup> S. A. Lloyd,<sup>5</sup> E. Kyro,<sup>7</sup> P. von der Gathen,<sup>8</sup> H. Claude,<sup>9</sup> J. Davies,<sup>10</sup> H. DeBacker,<sup>11</sup> H. Dier,<sup>12</sup> M. J. Molyneux,<sup>13</sup> and J. Sancho,<sup>14</sup>

Received 7 February 2001; revised 6 June 2001; accepted 6 July 2001; published 25 October 2002.

[1] In this paper we demonstrate the utility of the Polar Ozone and Aerosol Measurement (POAM) III data for providing semiglobal three-dimensional ozone fields during the Stratospheric Aerosol and Gas Experiment (SAGE) III Ozone Loss and Validation Experiment (SOLVE) winter. As a solar occultation instrument, POAM III measurements were limited to latitudes of 63°N to 68°N during the SOLVE campaign but covered a wide range of potential vorticity. Using established mapping techniques, we have used the relation between potential vorticity and ozone measured by POAM III to calculate three-dimensional ozone mixing ratio fields throughout the Northern Hemisphere on a daily basis during the 1999/2000 winter. To validate the results, we have extensively compared profiles obtained from ozonesondes and the Halogen Occultation Experiment to the proxy O<sub>3</sub> interpolated horizontally and vertically to the correlative measurement locations. On average, the proxy O<sub>3</sub> agrees with the correlative observations to better than ~5%, at potential temperatures below about 900 K and latitudes above about 30°N, demonstrating the reliability of the reconstructed O<sub>3</sub> fields in these regions. We discuss the application of the POAM proxy ozone profiles for calculating photolysis rates along the ER-2 and DC-8 flight tracks during the SOLVE campaign, and we present a qualitative picture of the evolution of polar stratospheric ozone throughout the winter.

INDEX TERMS: 0340

Atmospheric Composition and Structure: Middle atmosphere—composition and chemistry; 0341 Atmospheric Composition and Structure: Middle atmosphere—constituent transport and chemistry (3334); 0394

Atmospheric Composition and Structure: Instruments and techniques; 3337 Meteorology and Atmospheric Dynamics: Numerical modeling and data assimilation; KEYWORDS: POAM, ozone, reconstruction, SOLVE, potential vorticity, data assimilation

**Citation:** Randall, C. E., et al., Reconstruction of three-dimensional ozone fields using POAM III during SOLVE, *J. Geophys. Res.*, 107(D20), 8299, doi:10.1029/2001JD000471, 2002.

### 1. Introduction

[2] The Stratospheric Aerosol and Gas Experiment (SAGE) III Ozone Loss and Validation Experiment (SOLVE) campaign was designed to investigate the processes causing O<sub>3</sub> loss at high northern latitudes and to provide correlative data for validating SAGE III. One of the goals of SOLVE was to optimize the inference of O<sub>3</sub> loss from satellite observations, for those years when dedicated ground, balloon, and/or aircraft campaigns are not feasible. Although

the launch of SAGE III was unfortunately delayed, the Polar Ozone and Aerosol Measurement (POAM) III instrument, a satellite-based solar occultation instrument with latitude coverage similar to the planned SAGE III measurements, was (and still is) operational. During the SOLVE campaign, POAM III provided daily stratospheric profiles of ozone, water vapor, nitrogen dioxide, and aerosol extinction in the Northern Hemisphere (NH) from 63°N to 68°N with about 1 km vertical resolution. These measurements are being

<sup>1</sup>Laboratory for Atmospheric and Space Physics, University of Colorado, Boulder, Colorado, USA.

<sup>2</sup>Computational Physics, Inc., Springfield, Virginia, USA.

<sup>3</sup>Naval Research Laboratory, Washington, D. C., USA.

<sup>4</sup>Jet Propulsion Laboratory, Pasadena, California, USA.

<sup>5</sup>Applied Physics Laboratory, Johns Hopkins University, Laurel, Maryland, USA.

<sup>6</sup>Department of Chemistry and Biochemistry, University of Maryland, College Park, Maryland, USA.

<sup>7</sup>Finnish Meteorological Institute Sodankylä Observatory, Sodankylä, Finland.

<sup>8</sup>Alfred Wegener Institute for Polar and Marine Research, Potsdam, Germany.

<sup>9</sup>Hohenpeissenberg Observatory, Deutscher Wetterdienst, Hohenpeissenberg, Germany.

<sup>10</sup>Environment Canada, Downsview, Ontario, Canada.

<sup>11</sup>Royal Meteorological Institute of Belgium, Brussels, Belgium.

<sup>12</sup>Deutscher Wetterdienst Meteorological Observatory Lindenberg, Lindenberg, Germany.

<sup>13</sup>Meteorological Office, Wokingham, UK.

<sup>14</sup>Izana Atmospheric Observatory, Santa Cruz de Tenerife, Spain.

used to investigate the polar processes responsible for  $O_3$  loss during the 1999/2000 NH winter [e.g., Hoppel *et al.*, 2002; Bevilacqua *et al.*, 2002].

[3] It is now well established that the 1999/2000 NH polar vortex was unusually cold, with temperatures often below the threshold for forming polar stratospheric clouds [Manney and Sabutis, 2000].  $O_3$  decreases inside the polar vortex of  $0.04 \pm 0.01$  ppmv  $d^{-1}$  were observed in Microwave Limb Sounder (MLS) data from early February [Santee *et al.*, 2000], and  $O_3$  chemical loss of more than 70% by the end of March has been inferred from ozonesonde data at Ny Ålesund, Spitsbergen (79°N, 12°E) [Sinnhuber *et al.*, 2000]. Nevertheless, the precise mechanisms controlling the magnitude of the  $O_3$  loss have yet to be elucidated in detail. Ideally, a campaign such as SOLVE would be supported by global satellite measurements, with the ground-based, balloon, and aircraft measurements providing detailed but localized information, and the satellite providing measurements to place this information into a more global context. Although the Total Ozone Mapping Spectrometer (TOMS) instrument provides an excellent near-global map of column  $O_3$ , vertically resolved measurements are often preferable for mechanistic studies. Unfortunately, no instrument capable of providing global  $O_3$  profiles with high vertical resolution was operational throughout the SOLVE campaign (although the MLS was operational for 9 days in February and March [Santee *et al.*, 2000]).

[4] In an effort to improve this situation, we have reconstructed daily, semiglobal (NH only), vertically resolved  $O_3$  fields from the POAM data. The technique by which this was accomplished, which we refer to as potential vorticity (PV) mapping, was established more than a decade ago for use with Limb Infrared Monitor of the Stratosphere [Butchart and Remsberg, 1986] and ER-2 [Schoeberl *et al.*, 1989] data. This technique makes it possible, under certain conditions, to calculate mixing ratios over a much wider range of geographic locations than were actually observed. In this paper we describe the PV mapping technique as applied to the POAM III data, validate the results, and show how these results are useful for the SOLVE objectives.

[5] The premise behind the PV mapping technique is that PV is a conserved quantity during adiabatic transport, so it is often used as a tracer of atmospheric motions. Since  $O_3$  in the winter stratosphere is dynamically controlled, a single, well-defined relationship defines its correlation with PV across the polar vortex anywhere on a given potential temperature ( $\theta$ ) surface at any given point in time [e.g., Leovy *et al.*, 1985; Allaart *et al.*, 1993]. If this relationship is determined by measuring  $O_3$  over a sufficient range of PV/ $\theta$  space, it can thus be used to derive  $O_3$  mixing ratios at geographic locations outside the actual measurement field, as long as the PV and  $\theta$  values at those locations are known. The technique has been incorporated into studies of vortex processes in both hemispheres [Schoeberl *et al.*, 1989; Lait *et al.*, 1990; Manney *et al.*, 1998, 1999], and the underlying concepts have been used to improve satellite data intercomparisons [Manney *et al.*, 2001; Redaelli *et al.*, 1994]. This paper describes its first application with POAM III  $O_3$  data. POAM III routinely measured  $O_3$  profiles over a wide range of PV during the SOLVE campaign (see section 2). Taking

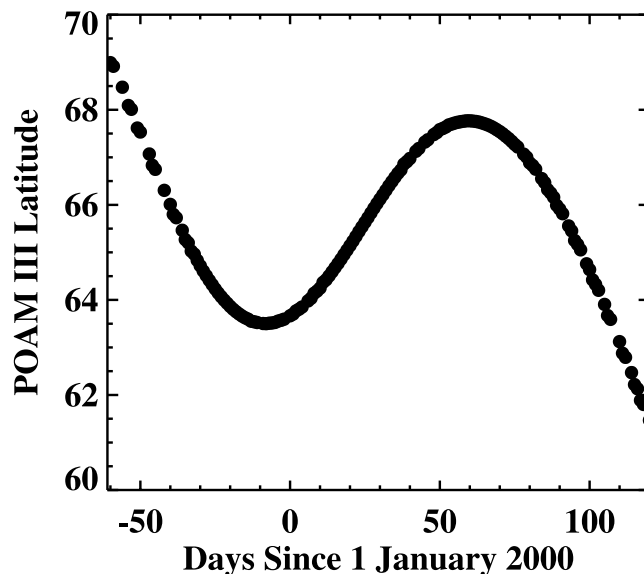


**Figure 1.** Latitudes of the NH POAM measurements from 1 November 1999 through 30 April 2000.

advantage of the PV analyses from the UK Meteorological Office (UKMO) [Swinbank and O'Neill, 1994], we were able to reconstruct  $O_3$  profiles on the NH UKMO grid, as described in section 3. We evaluated the NH gridded  $O_3$  “proxy” product by interpolating the profiles vertically and horizontally to the locations of correlative measurements, to which we compared the proxy profiles. These comparisons are described in section 4. The initial motivation for performing and validating the PV mapping with POAM III data during SOLVE was to derive  $O_3$  profiles above the SOLVE aircraft measurements. These profiles could then be used to determine solar flux transmissions for theoretical calculations of photolysis reaction rates. This application of the proxy  $O_3$  data is the subject of section 5.

## 2. POAM III Data

[6] Each day, approximately 15 POAM observations, separated by  $\sim 25^\circ$  in longitude, are made around a circle of approximately constant latitude in the Northern Hemisphere (NH) at local sunset. The average latitude of the observations on each day from 1 November 1999 through 30 April 2000 is shown in Figure 1. At each measurement location, POAM measures profiles of  $O_3$  ( $\sim 10$ –60 km), aerosol extinction at five wavelengths from 353 to 1020 nm ( $\sim 10$ –30 km),  $NO_2$  ( $\sim 20$ –40 km), and  $H_2O$  ( $\sim 10$ –45 km). In this paper we focus on the version 3.0 POAM III  $O_3$  data. Preliminary validation of an earlier version of POAM III  $O_3$  was described by Lucke *et al.* [1999]. More recent analyses with version 3.0 have been completed by Lumpe *et al.* [2002] and Randall *et al.* (Validation of POAM III  $O_3$ : Comparison to ozonesonde and satellite data, submitted to *Journal of Geophysical Research*, 2002) (hereinafter referred to as Randall *et al.* (submitted manuscript, 2002)). These show that on average, POAM III  $O_3$  profiles in the NH agree to better than 10% with correlative observations from 12 to 60 km.

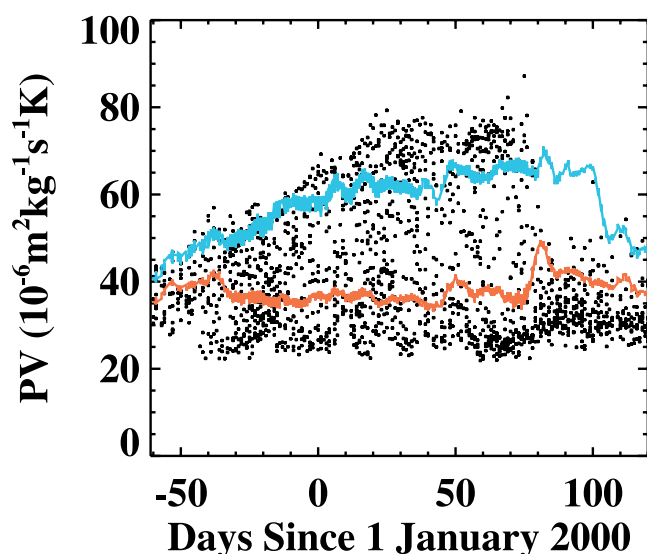


**Figure 2.** Potential vorticity of the NH POAM measurements from 1 November 1999 through 30 April 2000. The inner and outer boundaries of the vortex edge region are denoted in blue and red, respectively.

[7] Because the vortex is often displaced from the pole in the NH, POAM III makes measurements at a wide range of equivalent latitudes [Butchart and Remsberg, 1986] on a daily basis during the winter, even though the geographic latitude is essentially constant on a given day. For example, Figure 2 shows the PV on the 500 K potential temperature surface corresponding to every POAM measurement in the NH from 1 November 1999 through 30 April 2000. For this figure and elsewhere in the paper, we use UKMO PV analyses interpolated in time and space to the POAM measurement locations when necessary. The inner and outer vortex edge boundaries, as defined by Nash *et al.* [1996], are denoted in the plot. From late December through mid March, POAM sampled in the vortex core, on the vortex edge, and outside the vortex on a near-daily basis. It is this characteristic of the POAM measurements that allows the analysis described below.

[8] To illustrate how  $O_3$  changes with PV, a contour plot of the  $O_3$  field generated from measurements obtained by POAM over a 3-day period from 24–26 December 1999 is given in Figure 3. Maps such as this were provided to SOLVE campaign participants on a daily basis throughout the winter. At this particular time and latitude, measurement locations at longitudes of about  $330^\circ\text{E}$  to  $60^\circ\text{E}$  were inside the vortex (in-V), with longitudes near  $180^\circ$  well outside the vortex (out-V), and longitudes near  $120^\circ\text{E}$  and  $300^\circ\text{E}$  on the edge of the vortex (edge-V). This is quite typical for the vortex structure and location in the NH. Since  $O_3$  is in dynamical control at this time and latitude, mixing ratios follow the vortex structure. At all altitudes above about 500 K,  $O_3$  mixing ratios are significantly higher outside the vortex than inside; this results largely from transport of  $O_3$ -rich air from lower latitudes to the polar region outside the vortex [Randall *et al.*, 1995]. Inside the vortex, air parcels cannot mix as freely with the lower latitude air, so mixing ratios remain lower than outside the vortex. Near 450 K, where the vertical gradient

in the  $O_3$  profile is larger than at the higher altitudes,  $O_3$  mixing ratios inside the vortex are slightly higher than outside. This is due to enhanced diabatic descent inside the vortex. Because  $O_3$  mixing ratios increase with altitude here, air parcels descending inside the vortex to 450 K increase the  $O_3$  mixing ratios to values above those outside the vortex, where descent occurs less rapidly and with more horizontal mixing [e.g., Randall *et al.*, 1995; Manney *et al.*, 1995a, and references therein].

[9] Whereas Figure 3 illustrates the  $O_3$  variation with respect to the vortex that was observed in late December, Figure 4 presents the temporal variation in  $O_3$  that was observed at different locations with respect to the vortex over the course of the winter. This figure shows the daily average POAM III  $O_3$  mixing ratios segregated according to position with respect to the vortex (e.g., inside, outside, or on the edge) using the Nash *et al.* [1996] vortex definition. Although these observations were all acquired within the fairly narrow latitude band depicted in Figure 1, they illustrate some interesting features of the changes in vortex distribution of  $O_3$  during the winter at these latitudes. For instance, at 550 and 600 K, in-V mixing ratios are persistently lower than out-V mixing ratios, for the reasons stated above relating to poleward transport of high  $O_3$  mixing ratio air from lower latitudes. At 450 K in December, in-V  $O_3$  is more than 50% higher than out-V  $O_3$ . Again, this was explained above, and results from enhanced diabatic descent inside the vortex. However, in-V  $O_3$  mixing ratios at 450 K begin to decline steeply by mid February, so that by early March they are as low as out-V mixing ratios. This is the

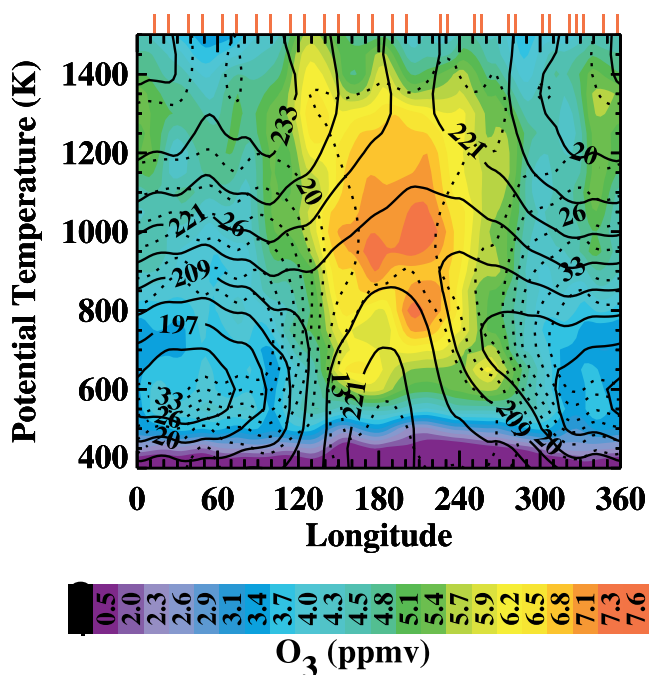


**Figure 3.** Representative contour map made from POAM III  $O_3$  measurements from 24 to 26 December 1999 at a latitude of  $63.5^\circ$ . The temperature (K) and modified PV ( $10^{-6} \text{ K m}^2 \text{ kg}^{-1} \text{ s}^{-1}$ ) [Lait, 1994] derived from UKMO data are superimposed as solid and dotted lines, respectively. POAM profile locations are given by the red marks above the top horizontal axis.



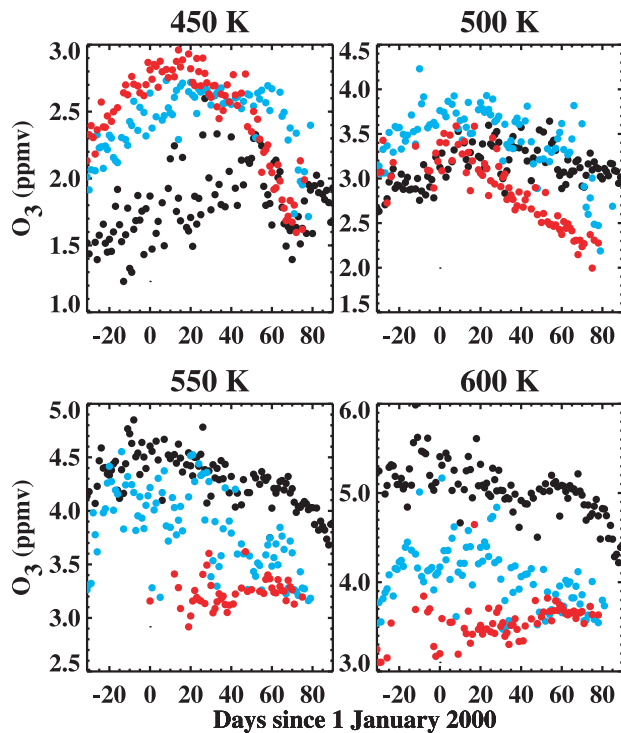


**Figure 4.** Daily average POAM III  $O_3$  mixing ratios inside the vortex (red), on the edge of the vortex (blue) and outside the vortex (black) from 1 December 1999 through 31 March 2000, at the potential temperatures noted in each panel.

signature of chemical  $O_3$  loss, and is discussed in more detail by Hoppel *et al.* [2002]. By early March, even edge-V  $O_3$  is declining at 450 K. Similar declines in in-V and edge-V  $O_3$  are also evident at 500 K. Another interesting feature is that until about mid January, edge-V mixing ratios at 500 K are higher than both in-V and out-V. We believe that this can be explained primarily by a variation across the edge of the vortex in the  $O_3$  profile vertical gradient near 500 K. Examination of POAM III profiles in October and November reveals that edge-V and out-V  $O_3$  mixing ratio profiles exhibited a steep gradient from 400 to 600 K. Enhanced diabatic descent on the edge of the vortex would have resulted in higher edge-V  $O_3$  than out-V, just as at 450 K. However, whereas in-V  $O_3$  mixing ratios followed a similarly steep gradient from 400 to 500 K, they were roughly constant near 3.0 ppmv or less above about 500 K. Thus enhanced diabatic descent inside the vortex produced little change in the in-V  $O_3$  mixing ratios at this time, resulting in edge-V  $O_3$  mixing ratios that were higher than both in-V and out-V. There may also be a contribution from faster diabatic descent along the edge of the vortex compared to inside. Reverse trajectory calculations performed elsewhere (G. Manney, private communication, 2001) showed that air parcels at 500 K on 5 January would have descended  $\sim 10$  K further on the edge of the vortex than inside during the preceding 40 days.

### 3. Method

[10] As mentioned above, the fact that PV is conserved during adiabatic transport allows us to use it to follow the

motion of tracers (such as  $O_3$  under many conditions) on isentropic surfaces. This concept can be applied to approximate  $O_3$  at geographic locations distant from actual measurements, as long as the measurements themselves adequately constrain the relationship between PV and  $O_3$ , and the PV values at the remote locations are well known [e.g., Schoeberl *et al.*, 1989]. As shown above, POAM III measurements span a wide range of PV values daily throughout the NH winter and clearly document variations in  $O_3$  expected from the changing PV. For every day during the SOLVE campaign, we thus calculated an analytic (quadratic) expression relating PV to  $O_3$  using the POAM III  $O_3$  profiles and the UKMO PV values interpolated in time and space to the POAM measurement locations. In practice, we actually used  $O_3$  and PV data corresponding to the 7-day interval centered on the day of interest. We found by trial and error that this interval length corresponded to the optimum balance for defining the PV/ $O_3$  relation. Including more days introduces error due to varying PV/ $O_3$  correlations, particularly in times of rapid vortex evolution. Including fewer days results in poorer statistics in general, the quadratic fits in these cases were qualitatively similar to the 7-day analyses but suffered from more noise. For each day during the SOLVE winter we then applied this relation to the daily 1200 UT NH UKMO PV field to generate proxy  $O_3$  mixing ratios on the same latitude/longitude grids as the UKMO data (for this work these grids spanned the NH in 2.5-degree increments in latitude and 3.75-degree increments in longitude).

[11] Our method is illustrated in Figure 5 for 1 January 2000 at 650 K. Figure 5a shows the POAM III  $O_3$  mixing ratios from 29 December through 4 January plotted against the UKMO PV interpolated to the POAM III measurement locations on the 650 K surface. For this altitude and time, high PV values correspond to the lowest values of  $O_3$ , and low PV values correspond to the highest values of  $O_3$ , since  $O_3$  outside the vortex is higher than inside, as discussed above. Superimposed on the data is a quadratic fit. We calculated a proxy  $O_3$  field for this day by multiplying the 650 K UKMO PV grid for 1 January by the quadratic coefficients defining the fit in Figure 5a. Figure 5b shows a contour map of the UKMO PV, clearly depicting the vortex as having an oval shape with its long axis oriented along  $90^\circ\text{E}$ – $270^\circ\text{E}$  longitude and its center displaced from the pole toward Greenland and Scandinavia. Over the 7-day period from 29 December to 4 January the POAM measurements spanned the latitude circle near  $63^\circ$ , in fairly regular longitude intervals of about five degrees. The measurements occurred well outside and inside the vortex, missing only the region with the very highest values of PV. The proxy  $O_3$  field, calculated from the PV field in Figure 5b and the quadratic coefficients defining the fit in Figure 5a, is plotted in Figure 5c. As expected from the monotonic PV/ $O_3$  relation in Figure 5a, the  $O_3$  field is essentially the reverse of the PV field, with low  $O_3$  inside the vortex, and high  $O_3$  outside the vortex.

[12] Extending this illustration to other days, Figure 6 shows the POAM III  $O_3$  mixing ratios at 500 K and quadratic PV/ $O_3$  fits for four different days during the SOLVE campaign. This figure illustrates the gradually changing PV/ $O_3$  relation over the course of the winter. Although similar information about the data can be derived

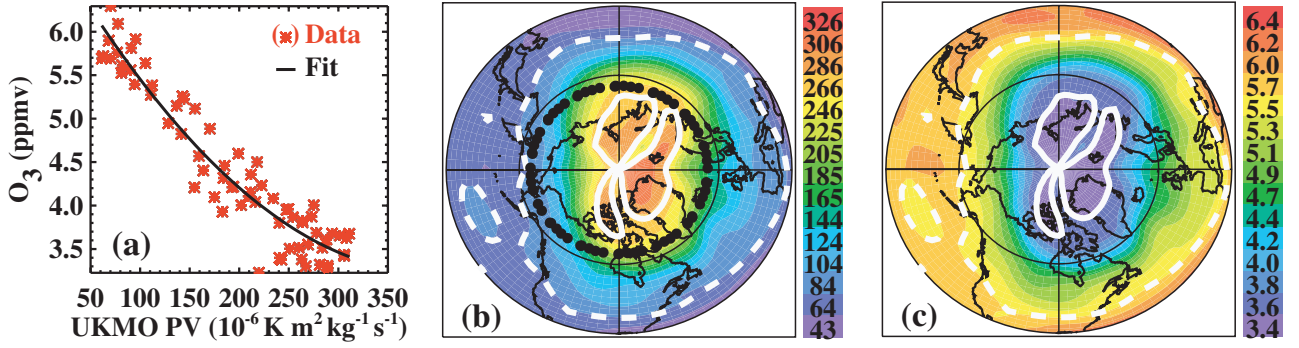


**Figure 5.** (a) POAM III  $O_3$  mixing ratios at 650 K from 29 December through 4 January 2000 (red asterisks), plotted against the UKMO PV interpolated in time and space to the POAM measurement locations. Superimposed is a quadratic fit to the data. (b) UKMO PV field on 1 January 2000 on the 650 K potential temperature surface. Latitude lines are drawn at  $30^\circ\text{N}$  and  $60^\circ\text{N}$ , and east longitudes increase counterclockwise from  $0^\circ$  on the right. POAM measurement locations from 29 December 1999 to 4 January 2000 are denoted by the black dots. Solid (dashed) white contours denote the geographic boundaries inside (outside) of which the PV values were higher (lower) than those sampled by POAM. (c) The proxy  $O_3$  field for 1 January 2000, calculated as described in the text. The color scales refer to (b) PV ( $10^{-6} \text{ m}^2 \text{ kg}^{-1} \text{ s}^{-1} \text{ K}$ ) and to (c)  $O_3$  mixing ratio (ppmv).

from Figure 4, we focus here on the quadratic fits to the data. The most salient point about this figure is that for all of these days, a quadratic fit appears to match the data quite well, on average. On 20 December, edge and in-V mixing ratios are higher than out-V, due to enhanced diabatic descent inside the vortex. The fit shows a slight enhancement of edge mixing ratios over in-V mixing ratios, but this is somewhat uncertain since, as shown in Figure 2, only a small fraction of the POAM measurements at this time occurred inside the inner edge of the vortex. Thus extrapolation of this quadratic to substantially higher values of PV is expected to be less certain than, for instance, extrapolation to lower values of PV. By the end of January, the enhancement of edge  $O_3$  mixing ratios over those both outside and inside the vortex is clear, the result of enhanced diabatic descent on the edge bringing down  $O_3$ -rich air. By late February the fits indicate mixing ratios inside the vortex that are significantly less than outside, a result expected only in the presence of chemical  $O_3$  loss. On 20 March, even though POAM sampled a wide range of PV, fewer points define the quadratic inside the vortex, suggesting higher uncertainty for the fit at this time.

[13] Applying the fits shown in Figure 6 to the UKMO PV fields, we generated the proxy  $O_3$  maps shown in Figure 7. Overall, these maps are consistent with the interpretation of the plots at the POAM latitudes discussed above. That is, areas of highest  $O_3$  in December through February form a collar near the vortex edge, where descent of  $O_3$ -rich air dominates. The areas of lowest  $O_3$  in February lie inside the vortex, and signify chemical  $O_3$  loss during the winter. On 20 March, the vortex was elongated and split into two areas of high PV (and relatively low  $O_3$ ), resulting in the double-lobed appearance to this map. These maps also illustrate, however, the potential for error when using the mapping technique to infer  $O_3$  at latitudes far from the original measurements. Consider, for instance, the map for 20 January 2000. The apparent intrusion of air with high  $O_3$  mixing ratios from the vortex edge to the pole near Greenland is an artifact due to anomalous structure in the UKMO PV field for this day.

Indeed, the proxy  $O_3$  mixing ratio at 500 K on 20 January, interpolated to the location of Eureka ( $79.9^\circ\text{N}$ ,  $-85^\circ\text{E}$ ), was higher by about 15% than the sonde measurement for that day.

[14] At the other extreme, the very low ( $\sim 2.2$  ppmv) proxy  $O_3$  mixing ratios on 20 January near  $80^\circ\text{N}$  latitude are also an artifact and are lower than actual measurements, for instance at Ny Ålesund (see section 4). These low mixing ratios result from an extrapolation of the PV/ $O_3$  relation to higher PV values and latitudes than were observed. The

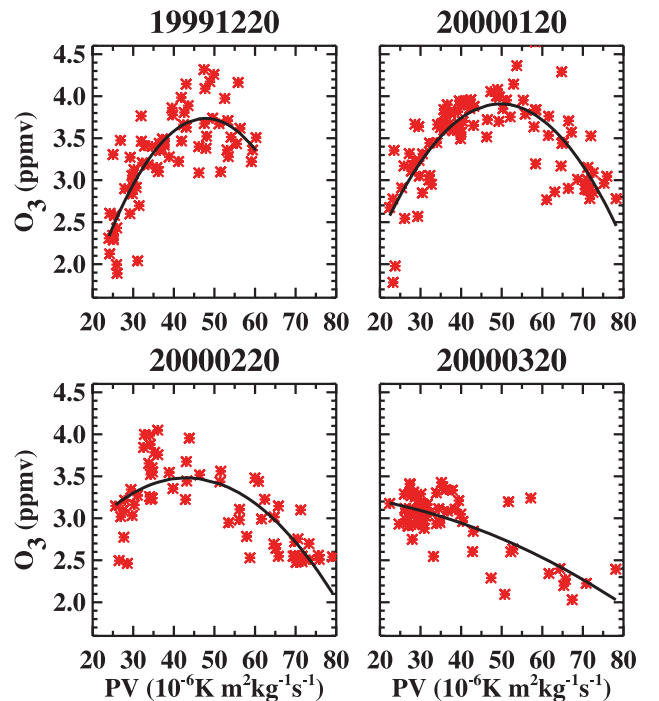


**Figure 6.** As in Figure 5a, but for the 500 K potential temperature level for the days noted in each panel.



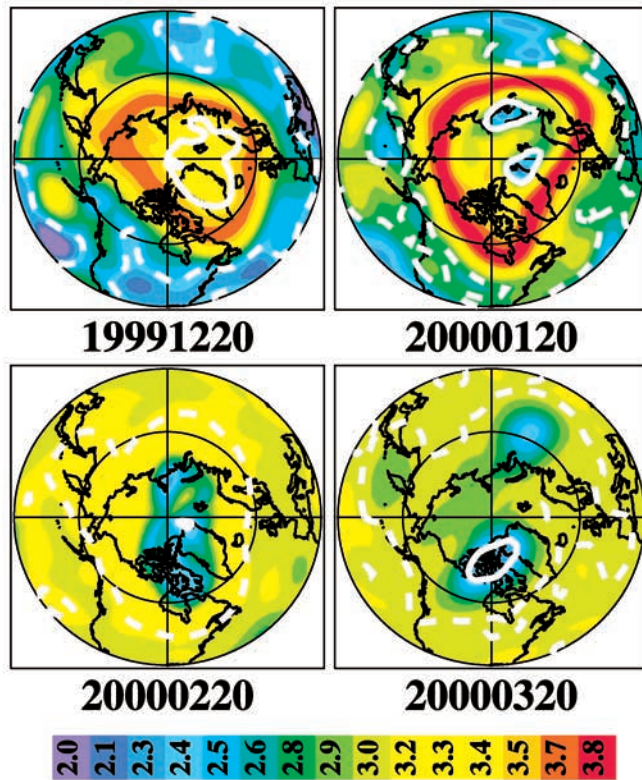


**Figure 7.** As in Figure 5c, but corresponding to the plots in Figure 6.

primary reason for this is that because of the dynamically induced higher  $O_3$  on the edge of the vortex, the mapping technique causes  $O_3$  to monotonically decrease at higher values of PV that are not sampled by POAM, rather than to level off to some extent inside the vortex. Using higher-order polynomials for the PV/ $O_3$  fits can alleviate this type of problem somewhat but introduces other artifacts into the analysis. This effect is exacerbated by the fact that the return of sunlight to the POAM measurement latitude ( $\sim 64^\circ\text{N}$ ) in January caused some chemical loss at 500 K (see Figure 4 and Hoppel *et al.* [2002]) inside the vortex. Even though such loss could not yet have occurred at the higher latitudes still in darkness, the mapping technique generalizes it to the entire vortex and in fact extrapolates to even lower  $O_3$  values at the higher PV values. In the next section we explore in detail the effects of such errors on the validity of the reconstructed fields.

#### 4. Validation of the Method

[15] To validate the PV mapping technique with POAM data, we have extensively compared the proxy  $O_3$  profiles generated using the method above to profiles obtained from balloon-based electrochemical concentration cell and Brewer-Mast ozonesondes and the Halogen Occultation Experiment (HALOE). Comparisons were made by interpolating the proxy  $O_3$  horizontally and vertically to the correlative measurement locations. These comparisons included locations both well north and well south of the actual POAM III measurement locations and both outside and inside the polar vortex. Ozonesonde profiles were

obtained from a sonde network operating within the framework of the SOLVE/Third European Stratospheric Experiment on Ozone (THESEO-2000) project. For this work we used data from 29 stations in Europe, North America, and Russia. Station locations and the number of profiles used from each are listed in Table 1. All data incorporated in our analysis have been quality controlled in real time during the SOLVE campaign by daily visual inspection of profiles. The time series data from Ny Ålesund (see below) have also passed a more rigorous, postmission quality control process. HALOE version 19  $O_3$  data were obtained from the HALOE home page (<http://haloedata.larc.nasa.gov/>). The  $O_3$  profiles were placed on potential temperature grids using the temperatures and pressures provided with the sonde (measured by radiosonde) and HALOE (obtained from the National Centers for Environmental Prediction) data sets.

[16] Figure 8 shows representative comparisons between individual ozonesonde profiles at three different locations and the proxy  $O_3$  profiles (determined by interpolation of the proxy  $O_3$  field on the UKMO grid to the sonde location). For this example we have chosen to show results from stations that were roughly  $14^\circ\text{N}$  (Ny Ålesund),  $17^\circ\text{S}$  (Hohenpeissenberg), and  $37^\circ\text{S}$  (Izana) of the POAM measurements. In general, the agreement with the sondes is excellent, with the proxy even capturing the steep lower stratospheric gradient in the  $O_3$  profile at Izana ( $28.4^\circ\text{N}$ ).

**Table 1.** Ozonesonde Stations Used in the Statistical Validation Analysis<sup>a</sup>

Station	Latitude	Longitude	Number of Comparisons
Aberystwyth	52.40	-4.10	5
Alert	82.50	-62.3	8
Andoya	69.30	16.11	6
Churchill	58.74	-94.00	6
De Bilt	52.10	5.18	7
Stonyplain	53.55	-114.	5
Eureka	79.99	-85.9	17
Gardermoen	60.11	11.04	3
Goose Bay	53.18	-60.2	4
Hohenpeissenberg	47.80	11.00	27
Izana	28.46	-16.2	2
Jaegersborg	55.77	12.53	1
Jokioinen	60.80	23.50	12
Lerwick	60.13	-1.18	22
Lindenberg	52.13	14.07	6
Legionowo	52.40	20.97	15
Ny Ålesund	78.93	11.95	29
Orland	63.42	9.24	14
Payame	46.80	6.95	30
Prague	50.02	14.45	12
Keflavik	63.97	-22.60	4
Resolute	74.71	-94.90	12
Salekhard	66.70	66.70	10
Scoresbysund	70.50	-22.00	10
Sodankyla	67.39	26.65	19
Thule	76.53	-68.70	5
Uccle	50.80	4.35	23
Valentia	51.93	-10.20	6
Yakutsk	62.03	129.60	5
Total			325

<sup>a</sup> The number of comparisons from each station that were included in the results shown in Figure 9 is listed in the last column. Profiles were obtained between 22 November 1999 and 1 February 2000.

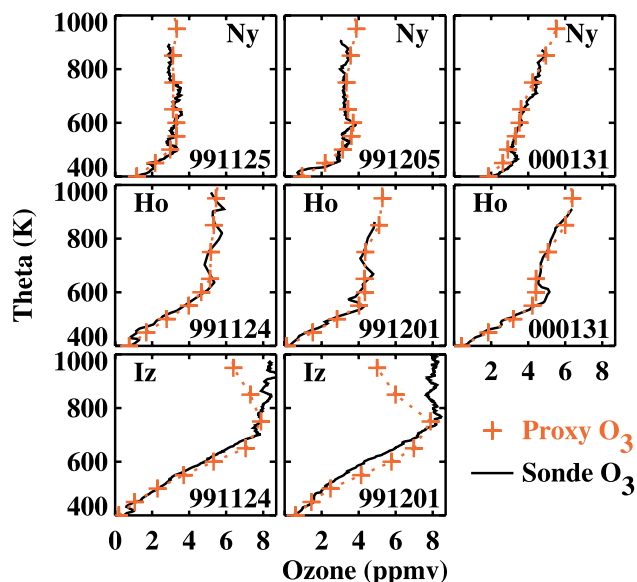


**Figure 8.** Representative examples of individual profile comparisons between the proxy O<sub>3</sub> interpolated to the sonde location (red, pluses) and the sonde profile (black) at Ny Ålesund (Ny), Hohenpeissenberg (Ho), and Izana (Iz), on the dates (yymmdd) shown in each panel.

The discrepancy above 700 K in the Izana comparisons is primarily due to the fact that at this low latitude and these high altitudes, O<sub>3</sub> is no longer a passive tracer.

[17] To quantify the sonde results, we have carried out a statistical analysis, calculating the average differences between the proxy and the sonde profiles for each of the measurements listed in Table 1. Figure 9 shows the average difference profile for these comparisons, as well as the individual differences and standard deviation of the mean (which is equivalent to the uncertainty in the mean). These results show that for the early to midwinter data included here, the proxy O<sub>3</sub> profiles on average agree with the sondes to better than 5% below about 800 K. This agreement is particularly noteworthy given the large range of sonde locations compared to the relatively localized POAM measurement latitudes. Approximately 4.4% of the comparisons shown in Figure 9 include proxy O<sub>3</sub> data that were derived from an extrapolation of the PV/O<sub>3</sub> quadratic fit beyond the range of PV values actually sampled by POAM (75 points out of 1720). The comparisons including these extrapolated points are fairly evenly distributed among the entire set of comparisons and do not significantly affect the overall averages.

[18] To better understand the latitude dependence of the quality of the proxy profiles, we have compared the proxy O<sub>3</sub> to more than 900 O<sub>3</sub> profiles measured by HALOE at the latitudes and times shown in Figure 10. The latitude dependence of the differences between HALOE and the proxy O<sub>3</sub> is shown in Figure 11 for four different potential temperature levels. These comparisons show that between 500 and 850 K the proxy O<sub>3</sub> generally agrees with the HALOE data remarkably well at latitudes poleward of 30°N (see below) but more poorly at equatorial latitudes. The larger differences at the lower latitudes probably have two causes. First, increasing uncertainty in the UKMO PV

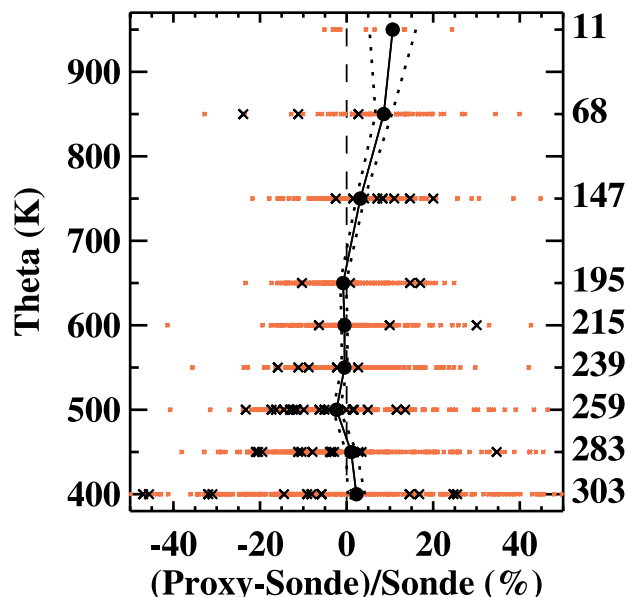


**Figure 9.** Statistical results for all ozonesonde comparisons between 22 November 1999 and 1 February 2000 shown as the average difference profile (solid line with dots) and the standard deviation of the mean (dotted lines), with the individual differences overplotted as red points (black crosses denote individual differences where the proxy O<sub>3</sub> was derived from an extrapolation of the PV/O<sub>3</sub> quadratic fit beyond the range of PV values actually sampled by POAM). The number of comparisons included at each potential temperature level is given on the right vertical axis.

field at these latitudes is likely to contribute to errors in the PV/O<sub>3</sub> analysis. Second, these latitudes correspond to PV values well outside the range sampled by POAM, where the quadratic relation may no longer hold (note that comparisons where the proxy O<sub>3</sub> was determined from an extrapolation of the PV/O<sub>3</sub> quadratic fit beyond the PV

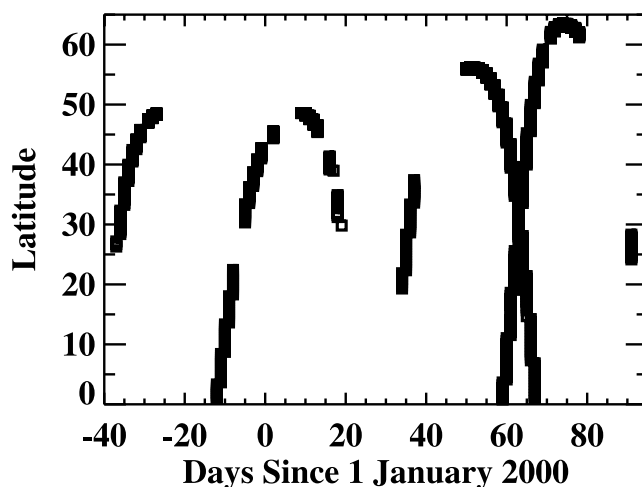


**Figure 10.** HALOE measurement latitudes in the NH during SOLVE from late November 1999 through March 2000.

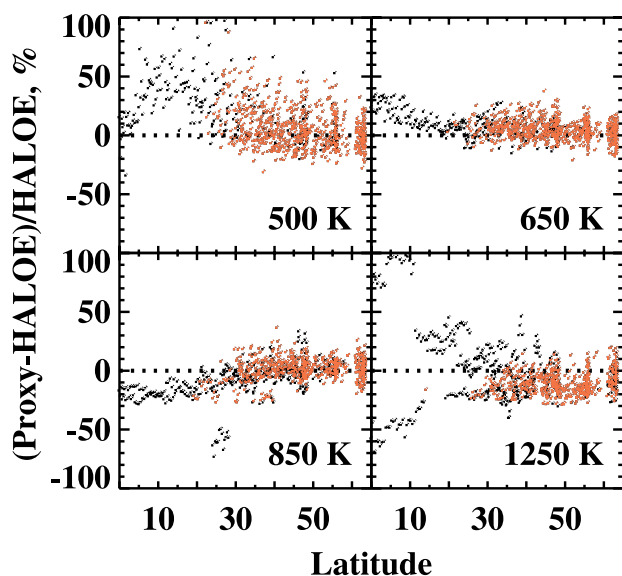


**Figure 11.** Latitude dependence of the differences between HALOE and the proxy  $O_3$  for events noted in Figure 10, at the potential temperature levels denoted in each panel. Comparisons including proxy  $O_3$  derived from extrapolation of the PV/ $O_3$  fit beyond the range of PV sampled by POAM are indicated in black; all other comparisons are indicated in red.

range sampled by POAM are denoted in black). At 650 K and above the results at the lower latitudes may also be affected by the fact that increasing sunlight will cause  $O_3$  to transition away from a dynamically controlled situation [Garcia and Solomon, 1985], increasing the error in the PV/ $O_3$  analysis. Although agreement is worse at 1250 K than at the lower altitudes, it is still quite reasonable poleward of  $30^\circ N$ .

[19] To quantify these comparisons, Figure 12 shows the statistical results for all events (724) poleward of  $30^\circ N$ . Comparisons including proxy  $O_3$  derived from an extrapolation of the PV/ $O_3$  quadratic fit beyond the PV range sampled by POAM constitute about 20% of the data points at latitudes poleward of  $30^\circ N$ ; their removal does not significantly alter the conclusions stated here. Like the sonde comparisons, agreement is impressive, with differences often less than 5% below 1100 K. The differences increase at the highest altitudes, most likely because of the lack of dynamical control at these altitudes as sunlight returns to the polar region. The large differences at 400 K in part reflect real differences between the POAM and HALOE data which have not yet been resolved (Randall et al., submitted manuscript, 2002). However, near 400 K the documented differences between POAM and HALOE are only at the 10% level, and cannot entirely explain either the average differences seen in Figure 12, or the marked increase in the variability of the comparisons at 400 K. We believe the deterioration in the comparisons at 400 K may result from increased mixing of air parcels at and below this altitude, where the effective diffusivity is generally higher than at higher altitudes [Haynes and Shuckburgh, 2000]. Variable small-scale mixing could change the PV/ $O_3$  relationship as a function of geographic location, so

that the fit derived from the POAM data would not necessarily apply to the location of the HALOE (or sonde) measurements. This would suggest that for the SOLVE winter the lower altitude limit for the PV mapping technique employed here is around 400–450 K. Confirming this speculation requires more investigation and is beyond the scope of this paper.

[20] To probe more deeply into the quality of the PV/ $O_3$  reconstruction at latitudes poleward of the POAM measurements, and to evaluate the proxy  $O_3$  in regions of chemical  $O_3$  loss, we have compared in detail the proxy  $O_3$  to ozonesonde measurements made at Ny Ålesund. At  $78.9^\circ N$  and  $12^\circ E$  this station is often located under the center of the NH vortex, where one might expect  $O_3$  loss to maximize. Indeed, as noted earlier,  $O_3$  loss of more than 70% during the SOLVE winter has been inferred above Ny Ålesund [Sinnhuber et al., 2000]. Figure 13 shows the evolution of  $O_3$  mixing ratios measured by sonde above Ny Ålesund at four different potential temperature levels between 450 and 750 K from late November through April. Superimposed are the proxy  $O_3$  values, interpolated to the latitude and longitude of Ny Ålesund. Throughout most of the winter, at all of these potential temperature levels, the agreement is remarkable, with mean differences ranging from about +5% to –7%. These results indicate that even at latitudes significantly poleward of the POAM measurements, and well inside the vortex, the PV mapping yields reasonable  $O_3$  values. In particular, the proxy field captures the variations in  $O_3$  at 450 K until early March and at 500 K until late March, including the decline caused by chemical loss processes. There are two noteworthy regions of disagreement. At 450 and 500 K, proxy  $O_3$  values at the end of January and beginning of February are generally somewhat lower than the sonde data. As discussed above with regard

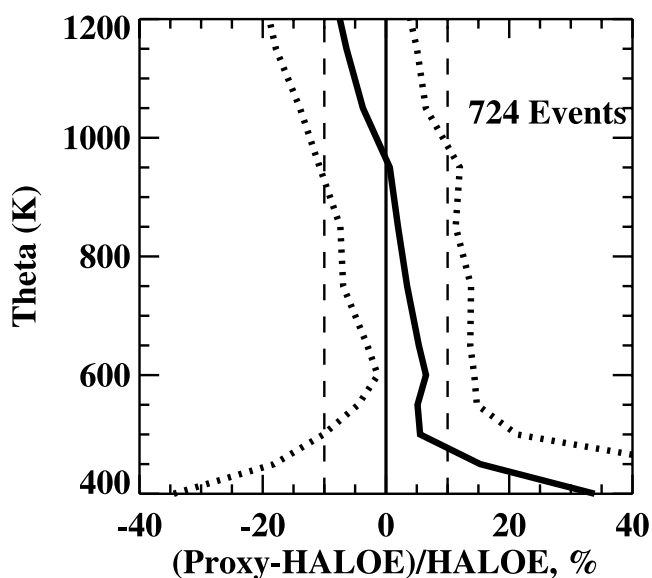


**Figure 12.** Statistical differences (heavy solid line) for events north of  $30^\circ N$  in the proxy-HALOE comparisons. Dotted lines are the standard deviation of the distribution. The standard deviations of the mean are approximately the thickness of the heavy solid line. Dashed lines are plotted at  $\pm 10\%$  for guidance.



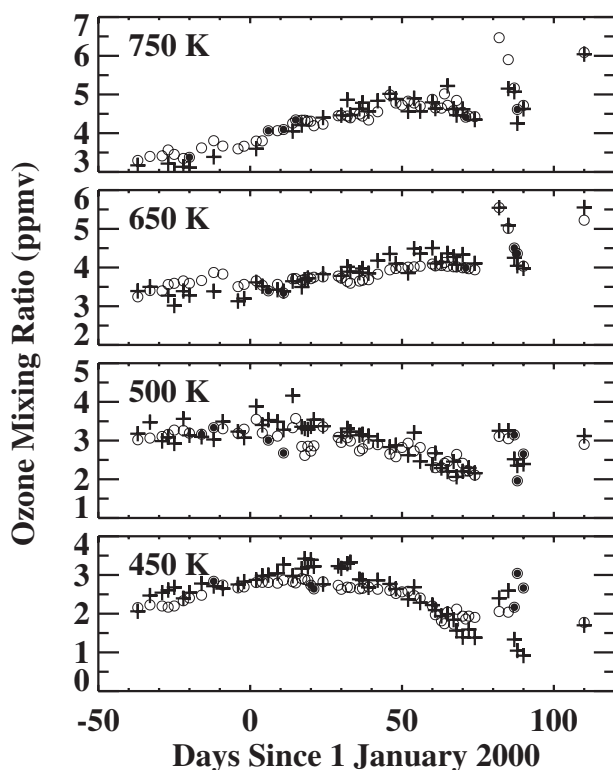


**Figure 13.** Evolution of  $O_3$  mixing ratios measured by ozonesonde over Ny Ålesund (pluses), at the different potential temperature levels noted in each panel, compared to the proxy  $O_3$  derived for the location of this station (open circles). Proxy  $O_3$  data derived from extrapolation of the  $PV/O_3$  quadratic fit beyond the range of  $PV$  sampled by POAM are denoted by the solid circles.

to Figure 7, this results from errors in the in- $V$  reconstruction stemming largely from the fact that the air parcels sampled by POAM have been exposed to more sunlight, and thus more chemical processing leading to  $O_3$  loss, than air over Ny Ålesund, even if they are at similar equivalent latitudes. In two cases, this is compounded by an extrapolation of the  $PV/O_3$  curve beyond the range of  $PV$  sampled by POAM. This comparison thus emphasizes the need for caution when interpreting the proxy  $O_3$  results in regions where geographic gradients due to photochemistry are significant, particularly if the proxy is derived from extrapolations beyond the sampled range of  $PV$ . The other notable disagreement occurs at 450 K near day 90, where proxy  $O_3$  is significantly higher than sonde  $O_3$ . At this time, POAM was sampling primarily on the edge of the vortex, and the mapping thus failed to capture the morphology of the substantial  $O_3$  loss that occurred at higher equivalent latitudes. Furthermore, the vortex was evolving rapidly at this time, increasing the uncertainty in the  $PV$  mapping analysis. Note, however, that the increase in  $O_3$  near day 80 (20 March), as the vortex shifted away from Ny Ålesund, was captured fairly well by the  $PV/O_3$  analysis.

[21] The comparisons presented here show that overall the proxy  $O_3$  profiles are in excellent agreement with correlative observations and can be used extensively for

scientific investigations. Caution is required, however, when there are significant errors in our knowledge of the  $PV/\theta$  fields, or in our knowledge of the  $PV/O_3$  relation. The latter error, which is the most prevalent, can arise for a number of different reasons. First, this will often result when the range of  $PV$  sampled by the instrument is too narrow to adequately extrapolate outside this range. Second, the  $PV/O_3$  relation may not follow closely enough the quadratic curve that we use to define it, instead being better defined by another analytic form. Third, if the  $PV/\theta$  field is changing rapidly (e.g., through diabatic processes), the  $PV/O_3$  relation defined by a 7-day period will average over these  $PV$  variations. Fourth, it may simply be inappropriate to assume a single (quadratic or otherwise)  $PV/O_3$  relation. This will be the case, for instance, when  $O_3$  is in photochemical control and is thus not expected to strictly correlate with  $PV$ . For example, we expect the analysis to work less well in the middle to upper stratosphere in summer, and also in the presence of the anticyclonic low  $O_3$  pockets that occur in the winter middle stratosphere [Manney *et al.*, 1995b; Nair *et al.*, 1998; Morris *et al.*, 1998]. For the latter situation there may be a perfectly valid quadratic that describes the  $PV/O_3$  relation everywhere except near the low  $O_3$  pockets, where the proxy  $O_3$  would overestimate the observed  $O_3$ . Note, however, that even in the presence of chemical changes, such as polar  $O_3$  loss, the mapping technique will produce valid results as long as  $O_3$  and  $PV$  are well correlated within the time period of the analysis, and as long as the observations fulfill the other requirements such as adequate sampling of the  $PV/\theta$  field (e.g., Figure 13).

## 5. Application of the Method

[22] The results above confirm the validity of the  $PV$  mapping technique for deriving proxy  $O_3$  values from the POAM III data at most times and locations during the NH winter poleward of  $30^\circ N$ . These results can be used for a variety of purposes and are particularly relevant in times (such as the SOLVE winter) when high vertical resolution, global,  $O_3$  measurements are lacking. In general, using the proxy  $O_3$  will improve analyses that rely on climatological profiles for lack of actual data. For instance, the proxy  $O_3$  data have been used to initialize calculations for investigations of  $O_3$  photochemical loss during the winter [Hoppel *et al.*, 2002] and can be used to improve satellite data retrievals which require a priori  $O_3$  profiles, such as those from the TOMS instrument. When combined with data from other instruments such as HALOE or SAGE, the analysis can be improved at the lower latitudes. We are currently using this strategy as one means of generating global stratospheric  $O_3$  fields for inclusion in the Navy's operational weather prediction system (NOGAPS [Hogan and Rosmund, 1991]). In this section we describe the application of POAM  $PV$  mapping results to calculations of photolysis rates relevant to SOLVE investigations.

[23] One of the primary goals of the SOLVE campaign was to investigate  $O_3$  loss processes using the numerous measurements of stratospheric species along the DC-8 and ER-2 flight paths. To put those measurements into the context of a detailed photochemistry scheme requires knowledge of the rate coefficients for the relevant photolytic

reactions; i.e., the  $j$  values. The  $j$  values can be calculated most directly if one measures the solar actinic flux that is transmitted through the atmosphere to the aircraft location from all directions, at the appropriate wavelengths. This is accomplished by the Scanning Actinic Flux Spectroradiometer (SAFS) instruments [Shetter and Müller, 1999] on the DC-8 for 15 molecules of interest. A more indirect determination of the  $j$  values is to measure the  $O_3$  column above the aircraft and to use this information to deduce the transmission through the atmosphere of the radiation responsible for the photolysis. The principal sources of overhead  $O_3$  information during previous ER-2 campaigns have been the in situ Composition and Photodissociative Flux Measurement (CPFM) [McElroy, 1995] and the TOMS satellite measurements (from which a climatological tropospheric column must be subtracted) [McPeters *et al.*, 1998]. A drawback to using these measurements, however, is that they become much less reliable or unavailable at high solar zenith angles (SZAs). Thus accurately determining  $O_3$  columns over the ER-2 at high SZAs was one of the primary motivating factors for applying the PV mapping technique to the POAM III data.

[24] The POAM III reconstructed  $O_3$  fields have been used to create consistent  $j$  value data sets for the entire campaign, independent of limitations at high SZAs. This has been done independently by two different groups, at the Applied Physics Laboratory (APL) and at the Jet Propulsion Laboratory (JPL). In order to calculate accurate  $j$  values, it is necessary that the reconstructed  $O_3$  at and above the aircraft flight track be accurate. The validation discussion above showed that statistically the reconstructed profiles interpolated to ozonesonde and HALOE

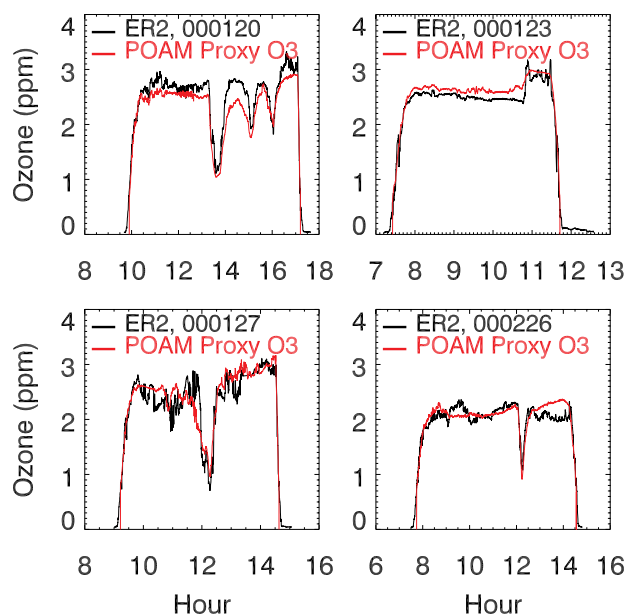


**Figure 14.** Comparison of the reconstructed  $O_3$  interpolated to the ER-2 flight location (red) and the in situ measurements from the ozone photometer on board the ER-2 (black) during the flight on the date (yyymmdd) noted in each panel. The sharp dips in the  $O_3$  measurements correspond to rapid altitude changes by the ER-2.

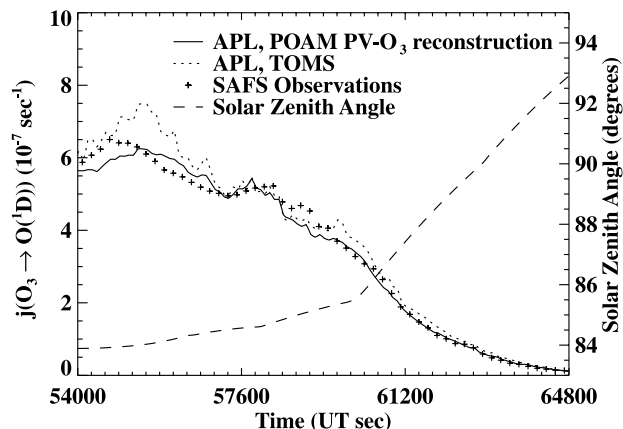


**Figure 15.** Comparison of  $O_3$  photolysis  $j$  values determined by the APL group based on the POAM reconstructed  $O_3$  (solid) and the TOMS total column measurements (dotted) to calculations based on SAFS actinic flux observations (pluses) for the DC-8 flight on 3 March 2000. The SZA variation along the flight track is denoted by the dashed line.

measurement locations compared very well to the observations. We investigated the reliability of the PV mapping results for determining  $O_3$  at the aircraft location by comparing the proxy  $O_3$  to in situ  $O_3$  measurements from the ozone photometer on board the ER-2 [Proffitt and McLaughlin, 1983; Richard *et al.*, 2001]. For these comparisons, some representative examples of which are shown in Figure 14, the proxy  $O_3$  was interpolated horizontally and vertically to the ER-2 flight tracks. Figure 14 reveals excellent agreement between the proxy  $O_3$  and ER-2 observations, even during the rapid altitude changes (dips) of the aircraft, as expected from the comparisons shown above.

[25] To illustrate the reliability of the  $j$  value calculations themselves, Figure 15 compares the APL calculations [Swartz *et al.*, 1999] appropriate for the DC-8 flight on 3 March 2000 to the  $j$  values derived using actinic flux measurements from the SAFS measurement, for the  $O_3 \rightarrow O(^1D)$  reaction. The  $j$  values derived from the POAM reconstruction analysis match those derived from the SAFS measurements quite well, generally agreeing to within 10% or better. Also shown are the  $j$  values determined using TOMS measurements of total ozone. These also match the SAFS determinations well, although not quite as well as the POAM-based calculations for this particular flight. It should be noted that for the TOMS calculations, climatological  $O_3$  profiles were scaled to the TOMS total column, so that the  $O_3$  column below the DC-8 could be subtracted off. Likewise, climatological profiles were used to extend the POAM measurements down to the DC-8 flight altitude. When averaged over the entire campaign, the APL(TOMS) calculations of  $j(O_3)$  at  $SZA > 85^\circ$  exceeded determinations based on the SAFS data by  $\sim 13 \pm 3\%$ . The APL(POAM) calculations on average agreed better with the SAFS determinations, exceeding them by only  $3 \pm 2\%$ . With regard to these results, however, it is important to note that the TOMS

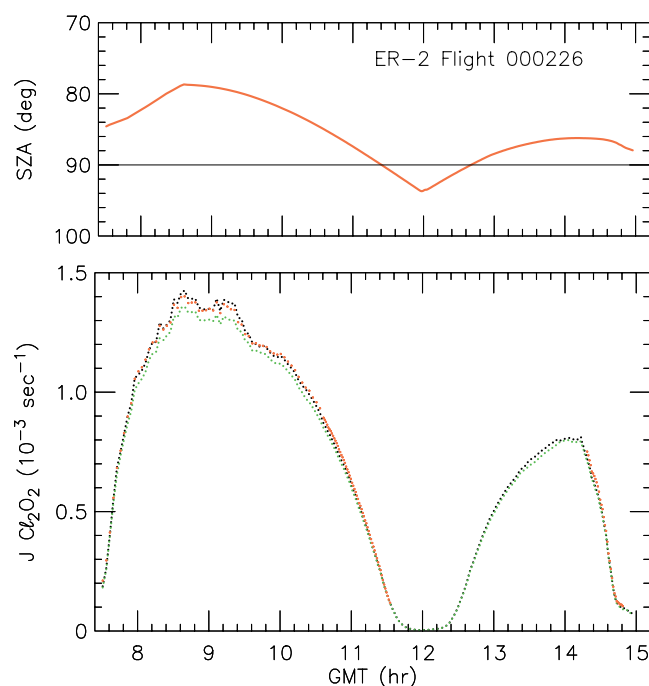


**Figure 16.** Comparison of  $\text{Cl}_2\text{O}_2$  photolysis  $j$  values determined by the JPL group based on the POAM reconstructed  $\text{O}_3$  (green) and the POAM reconstructed  $\text{O}_3$  scaled to the TOMS measurements (black), to calculations based on the CPFM data (red) for the ER-2 flight on 26 February 2000. The SZAs of the measurements are noted in the top panel.

total  $\text{O}_3$  retrieval has not been optimized for the high latitudes and SZAs encountered during the SOLVE campaign. At lower SZAs, APL(TOMS) and APL(POAM) provided more comparable levels of agreement with SAFS.

[26] Figure 16 demonstrates the utility of the  $j$  value calculations based on the POAM reconstruction for ER-2 flights. In this figure we compare JPL  $j$  value calculations for the photolysis of  $\text{Cl}_2\text{O}_2$  based on column  $\text{O}_3$  determined from the POAM reconstruction and the CPFM measurements. We show two different derivations for the POAM reconstruction, including calculations based solely on the POAM proxy data, as well as calculations based on the proxy data scaled to the TOMS total column  $\text{O}_3$ . For the latter case, the reconstructed  $\text{O}_3$  profiles are scaled such that the total column abundance of the proxy profile, which is extended below the POAM measurements with a climatological profile, matches the TOMS total column. For this case, the proxy, scaled proxy, and CPFM  $j$  value determinations match quite well throughout most of the flight. However, at the highest SZAs, between  $\sim 11.5$  and 14 UT, the CPFM values are unavailable. Thus the proxy determination serves to fill in this time gap. Similar results are seen for other flights and other  $j$  values: in general, there is good agreement between estimates of overhead ozone, and thus  $j$  values, based on the POAM reconstruction and the CPFM data, for SZA less than about  $85^\circ$ . For the largest SZA, however, the reconstruction with POAM data provides a more accurate method of determining  $j$  values than simply

relying on climatological data, as has been the practice in the past.

## 6. Summary

[27] For each day during the 1999/2000 winter we have used the relation between PV and  $\text{O}_3$  mixing ratio to calculate semiglobal (NH only) three-dimensional  $\text{O}_3$  fields. The work presented here represents the first demonstration of the PV mapping technique applied to solar occultation measurements at high equivalent latitudes over the course of an entire winter. We have extensively compared the proxy  $\text{O}_3$  so generated to profiles obtained from ozonesondes and HALOE. Comparisons were made by interpolating the proxy  $\text{O}_3$  horizontally and vertically to the correlative measurement locations. These comparisons included locations both well north and well south of the actual POAM III measurement locations, and both outside and inside the polar vortex. On average, the proxy  $\text{O}_3$  agrees with the correlative observations to better than  $\sim 5\%$ , at potential temperatures below about 900 K, and at latitudes above about  $30^\circ\text{N}$  (i.e., in the region where  $\text{O}_3$  is dynamically controlled). These results demonstrate the reliability of the reconstructed global fields using the PV mapping technique. The POAM III proxy ozone fields have been used to estimate  $\text{O}_3$  profiles for the computation of photolysis rates along the SOLVE aircraft flight tracks.

[28] Finally, Figure 17 shows the proxy fields at 500 K throughout the SOLVE winter in 5-day increments. This figure graphically illustrates the changing ozone field as dynamical and chemical processes perturb the polar region over the course of the winter. Air descending in and on the edge of the vortex causes  $\text{O}_3$  mixing ratios to increase at 500 K and is responsible for the ring at the edge of the vortex that is so prominent in most of the panels. Persistent chemical  $\text{O}_3$  loss inside the vortex begins in late January at POAM latitudes and continues through March, as indicated by the transition toward the blue end of the color scale. Toward the end of March the vortex begins to break down at 500 K, and the two pockets of low ozone on 21 March coincide with the two branches of the vortex at this time. Even as late as 20 April, there are persistently low  $\text{O}_3$  mixing ratios coinciding with the highest PV values, presumably remnants of the low- $\text{O}_3$  regions which formed during the winter inside the vortex. As noted above, detailed interpretation of the proxy fields requires caution when mechanisms responsible for ozone variability depend on factors other than equivalent latitude. In spite of this caveat, and other potential errors discussed above, the proxy fields illustrate the versatility and applicability of the solar occultation observations for  $\text{O}_3$  loss investigations. Furthermore, by presenting a three-dimensional picture of the changing Arctic  $\text{O}_3$ , they provide information easily accessible to the general public. The proxy fields present a qualitative picture of semiglobal, vertically resolved  $\text{O}_3$  variations throughout the winter in the lower stratosphere, a picture that is not directly available from any of the currently operational satellite instruments. This method is easily extended to other winters measured by POAM II and POAM III. Ideally, POAM III data will be combined with HALOE or SAGE II to improve results at the lower latitudes, and with SAGE III measurements to improve PV sampling at the highest latitudes.



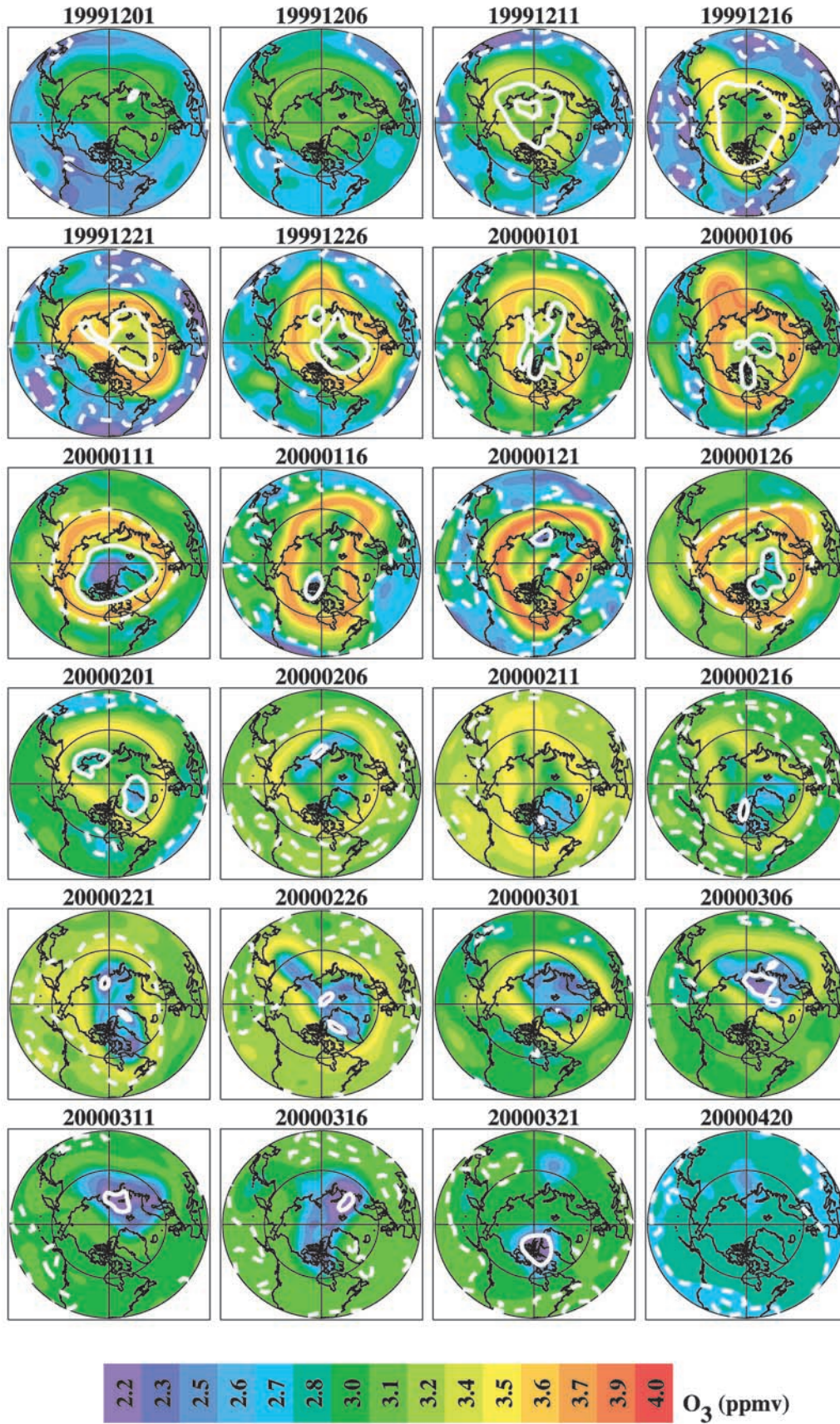


**Figure 17.** Proxy O<sub>3</sub> maps on the 500 K potential temperature level, as in Figure 7, for the dates shown in each panel. Note that the final panel succeeds the previous one by 1 month.

[29] **Acknowledgments.** This work was supported by NASA grant N00014-97-1-G018 and by the NASA Scientific Data Purchase program through contract NAS13-99031. We thank G. Manney for helpful discussions, R. Shetter for providing the SAFS data, and M. Rex for providing easy access to ozonesonde data during the SOLVE campaign. Version 3.0 POAM III data can be obtained from the NASA Langley Research Center EOSDIS Distributed Active Archive Center. We would like to acknowledge the following providers of ozonesonde data: V. Dorokhov (Central Aerological Observatory, Russia), M. Gil (Icelandic Meteorological Office and Instituto Nacional de Técnica Aeroespacial), I. S. Mikkelsen (Danish Meteorological Institute; Jaegersborg, Scoresbysund, Thule), Z. Litynska (IMWM, Legionowo), R. Stubi (Meteoswiss/Payerne), T. Turunen (Finnish Meteorological Institute, Sodankylä), and G. Vaughan (University of Wales, Aberystwyth).

## References

- Allaart, M. A. F., H. Kelder, and L. C. Heijboer, On the relation between ozone and potential vorticity, *Geophys. Res. Lett.*, **20**, 811–814, 1993.
- Bevilacqua, R. M., et al., Observations and analysis of PSCs detected by POAM III during the 1999/2000 Northern Hemisphere winter, *J. Geophys. Res.*, **107**, doi:10.1029/2001JD00477, in press, 2002.
- Butchart, N., and E. E. Remsberg, The area of the stratospheric polar vortex as a diagnostic for tracer transport on an isentropic surface, *J. Atmos. Sci.*, **43**, 1319–1339, 1986.
- Garcia, R. R., and S. Solomon, The effect of breaking gravity waves on the dynamics and chemical composition of the mesosphere and lower thermosphere, *J. Geophys. Res.*, **90**, 3850–3868, 1985.
- Haynes, P., and E. Shuckburgh, Effective diffusivity as a diagnostic of atmospheric transport, I, Stratosphere, *J. Geophys. Res.*, **105**, 22,777–22,794, 2000.
- Hogan, T., and T. Rosmund, The description of the Navy Operational Global Atmospheric Prediction Systems spectral forecast model, *Mon. Weather Rev.*, **119**, 1786–1815, 1991.
- Hoppel, K. W., et al., POAM III observations of Arctic ozone loss for the 1999/2000 winter, *J. Geophys. Res.*, **107**(D20), doi:10.1029/2001JD00476, 2002.
- Lait, L. R., An alternative form for potential vorticity, *J. Atmos. Sci.*, **51**, 1754–1759, 1994.
- Lait, L. R., et al., Reconstruction of O<sub>3</sub> and N<sub>2</sub>O fields from ER-2, DC-8, and balloon observations, *Geophys. Res. Lett.*, **17**, 521–524, 1990.
- Leovy, C. B., C.-R. Sun, M. H. Hitchman, E. E. Remsberg, J. M. Russell III, L. L. Gordley, J. C. Gille, and L. V. Lyjak, Transport of ozone in the middle stratosphere: Evidence for planetary wave breaking, *J. Atmos. Sci.*, **42**, 230–244, 1985.
- Lucke, R. L., et al., The Polar Ozone and Aerosol Measurement (POAM) III instrument and early validation results, *J. Geophys. Res.*, **104**, 18,757–18,799, 1999.
- Lumpe, J. D., et al., Comparison of POAM III ozone measurements with correlative aircraft and balloon data during SOLVE, *J. Geophys. Res.*, **107**, doi:10.1029/2001JD000472, in press, 2002.
- Manney, G. L., and J. L. Sabutis, Development of the polar vortex in the 1999–2000 Arctic winter stratosphere, *Geophys. Res. Lett.*, **27**, 2589–2592, 2000.
- Manney, G. L., L. Froidevaux, J. W. Waters, and R. W. Zurek, Evolution of microwave limb sounder ozone and the polar vortex during winter, *J. Geophys. Res.*, **100**, 2953–2972, 1995a.
- Manney, G. L., et al., Formation of low ozone pockets in the middle stratosphere anticyclone during winter, *J. Geophys. Res.*, **100**, 13,939–13,950, 1995b.
- Manney, G. L., J. C. Bird, D. P. Donovan, T. J. Duck, J. A. Whiteway, S. R. Pal, and A. I. Carswell, Modeling ozone laminae in ground-based Arctic wintertime observations using trajectory calculations and satellite data, *J. Geophys. Res.*, **103**, 5797–5814, 1998.
- Manney, G. L., H. A. Michelsen, M. L. Santee, M. R. Gunson, F. W. Irion, A. E. Roche, and N. J. Livesey, Polar vortex dynamics during spring and fall diagnosed using trace gas observations from the Atmospheric Trace Molecule Spectroscopy instrument, *J. Geophys. Res.*, **104**, 18,841–18,866, 1999.
- Manney, G. L., et al., Comparison of satellite ozone observations in coincident air masses in early November 1994, *J. Geophys. Res.*, **106**, 9923–9943, 2001.
- McElroy, C. T., A spectroradiometer for the measurement of direct and scattered solar irradiance from on board the NASA ER-2 high-altitude research aircraft, *Geophys. Res. Lett.*, **22**, 1361–1364, 1995.
- McPeters, R., et al., Earth Probe Total Ozone Mapping Spectrometer (TOMS) data products user's guide, *Rep. NASA/TP-1998-206895*, NASA Goddard Space Flight Cent., Greenbelt, Md., 1998.
- Morris, G. A., S. R. Kawa, A. R. Douglass, M. R. Schoeberl, L. Froidevaux, and J. Waters, Low-ozone pockets explained, *J. Geophys. Res.*, **103**, 3599–3610, 1998.
- Nair, H., M. Allen, L. Froidevaux, and R. W. Zurek, Localized rapid ozone loss in the northern winter stratosphere: An analysis of UARS observations, *J. Geophys. Res.*, **103**, 1555–1571, 1998.
- Nash, E. R., P. A. Newman, J. E. Rosenfield, and M. R. Schoeberl, An objective determination of the polar vortex using Ertel's potential vorticity, *J. Geophys. Res.*, **101**, 9471–9478, 1996.
- Proffitt, M. H., and R. J. McLaughlin, Fast-response dual-beam UV absorption ozone photometer suitable for use on stratospheric balloons, *Rev. Sci. Instrum.*, **54**, 1719–1728, 1983.
- Randall, C. E., et al., Preliminary results from POAM II: Stratospheric ozone at high northern latitudes, *Geophys. Res. Lett.*, **22**, 2733–2736, 1995.
- Redaelli, G., et al., UARS MLS O<sub>3</sub> soundings compared with lidar measurements using the conservative coordinates reconstruction technique, *Geophys. Res. Lett.*, **21**, 1535–1538, 1994.
- Richard, E. C., Severe chemical ozone loss inside the Arctic polar vortex during winter 1999–2000 inferred from in situ airborne measurements, *Geophys. Res. Lett.*, **28**, 2197–2200, 2001.
- Santee, M. L., G. L. Manney, N. J. Livesey, and J. W. Waters, UARS Microwave Limb Sounder observations of denitrification and ozone loss in the 2000 Arctic winter, *Geophys. Res. Lett.*, **27**, 3213–3216, 2000.
- Schoeberl, M. R., et al., Reconstruction of the constituent distribution and trends in the Antarctic polar vortex from ER-2 flight observations, *J. Geophys. Res.*, **94**, 16,815–16,845, 1989.
- Shetter, R. E., and M. Müller, Photolysis frequency measurements using actinic flux spectroradiometry during the PEM-Tropics mission: Instrumentation description and some results, *J. Geophys. Res.*, **104**, 5647–5661, 1999.
- Sinnhuber, B.-M., et al., Large loss of total ozone during the Arctic winter of 1999/2000, *Geophys. Res. Lett.*, **27**, 3473–3476, 2000.
- Swartz, W. H., S. A. Lloyd, T. L. Kusterer, D. E. Anderson, C. T. McElroy, and C. Midwinter, A sensitivity study of photolysis rate coefficients during POLARIS, *J. Geophys. Res.*, **104**, 26,725–26,735, 1999.
- Swinbank, R., and A. O'Neill, A stratosphere-troposphere data assimilation system, *Mon. Weather Rev.*, **122**, 686–702, 1994.

R. M. Bevilacqua and K. W. Hoppel, Naval Research Laboratory, Code 7220, Bldg. 2, 4555 Overlook Ave., SW, Washington, DC, 20375-5320, USA. (bevilacqua@nrl.navy.mil; karl.hoppel@nrl.navy.mil)

H. Claude, Hohenpeissenberg Observatory, Deutscher Wetterdienst, Albin-Schwaiger-Weg 10, 82383, Hohenpeissenberg, Germany. (hans.claude@dwd.de)

J. Davies, Environment Canada, 4905 Dufferin Street, Downsview, Ontario, Canada M3H 5T4. (jonathan.davies@ec.gc.ca)

H. DeBacker, Royal Meteorological Institute of Belgium, Ringlaan 3, B-1180, Brussels, Belgium. (hugo.debacker@oma.be)

H. Dier, DWD Meteorological Observatory Lindenberg, Am Observatorium 12, 15864 Lindenberg, Germany. (horst.dier@dwd.de)

M. D. Fromm and J. D. Lumpe, Computational Physics, Inc., 8001 Braddock Road, Suite 210, Springfield, VA 22151, USA. (fromm@poamb.nrl.navy.mil; lumpe@cpi.com)

E. Kyro, FMI Sodankylä Observatory, Tähteläntie 71, FIN-99600, Sodankylä, Finland. (esko.kyro@fmi.fi)

S. A. Lloyd and W. H. Swartz, Applied Physics Laboratory, Johns Hopkins University, 11100 Johns Hopkins Rd., Laurel, MD 20723-6099, USA. (steven\_lloyd@jhuapl.edu; bill.swartz@jhuapl.edu)

M. J. Molyneux, Meteorological Office, Beaufort Park, Easthampstead, Wokingham, Berkshire, RG40 3DN, UK. (mjmolyneux@meto.gov.uk)

C. E. Randall, Laboratory for Atmospheric and Space Physics, University of Colorado, Campus Box 392, Boulder, CO 80309-0392, USA. (cora.randall@lasp.colorado.edu)

R. J. Salawitch, Jet Propulsion Laboratory, MS 183-301, 4800 Oak Grove Dr., Pasadena, CA 91109, USA. (rjs@caesar.jpl.nasa.gov)

J. Sancho, Izana Atmospheric Observatory, La Marina, 20, P.O. Box 880, Santa Cruz de Tenerife, Spain. (jsancho@inm.es)

P. von der Gathen, Alfred Wegener Institute for Polar and Marine Research, Research Site Potsdam, Telegrafenberg A43, D-14473, Potsdam, Germany. (gathen@awi-potsdam.de)